

# Evaluation of [ $^{11}\text{C}$ ]hemicholinium-15 and [ $^{18}\text{F}$ ]hemicholinium-15 as new potential PET tracers for the high-affinity choline uptake system in the heart

Mingzhang Gao,<sup>a</sup> Michael A. Miller,<sup>a</sup> Timothy R. DeGrado,<sup>a</sup> Bruce H. Mock,<sup>a</sup> John C. Lopshire,<sup>b</sup> Joshua G. Rosenberger,<sup>b</sup> Cristian Dusa,<sup>b</sup> Mithilesh Kumar Das,<sup>b</sup> William J. Groh,<sup>b</sup> Douglas P. Zipes,<sup>b</sup> Gary D. Hutchins<sup>a</sup> and Qi-Huang Zheng<sup>a,\*</sup>

<sup>a</sup>Department of Radiology, Indiana University, Indianapolis, IN 46202, USA

<sup>b</sup>Krannert Institute of Cardiology, Indiana University, Indianapolis, IN 46202, USA

Received 9 October 2006; revised 31 October 2006; accepted 8 November 2006

Available online 10 November 2006

**Abstract**—[ $^{11}\text{C}$ ]Hemicholinium-15 ([ $^{11}\text{C}$ ]HC-15) and [ $^{18}\text{F}$ ]hemicholinium-15 ([ $^{18}\text{F}$ ]HC-15) have been synthesized as new potential PET tracers for the heart high-affinity choline uptake (HACU) system. [ $^{11}\text{C}$ ]HC-15 was prepared by *N*-[ $^{11}\text{C}$ ]methylation of the appropriate precursor, 4-methyl-2-phenyl-morpholin-2-ol, using [ $^{11}\text{C}$ ]CH<sub>3</sub>OTf in 55–70% radiochemical yield decay corrected to end of bombardment (EOB) and 2–3 Ci/ $\mu\text{mol}$  specific activity at end of synthesis (EOS). [ $^{18}\text{F}$ ]HC-15 was prepared by *N*-[ $^{18}\text{F}$ ]fluoromethylation of the precursor using [ $^{18}\text{F}$ ]FCH<sub>2</sub>OTf in 20–30% radiochemical yield decay corrected to EOB and >1.0 Ci/ $\mu\text{mol}$  specific activity at EOS. The biodistribution of both compounds was determined in rats at 20 min post-intravenous injection, and the results show the heart region uptakes  $1.32 \pm 0.75\%$ ID/g in R-ventricle for [ $^{11}\text{C}$ ]HC-15 and  $1.28 \pm 0.81\%$ ID/g in L-ventricle for [ $^{18}\text{F}$ ]HC-15, respectively. The dynamic PET imaging studies of [ $^{11}\text{C}$ ]HC-15 in rats were acquired 60 min post-intravenous injection of the tracer using the IndyPET-II scanner. For the blocking experiments, the rats were intravenously pretreated with 3.0 mg/kg of unlabeled HC-15 prior to [ $^{11}\text{C}$ ]HC-15 injection. [ $^{11}\text{C}$ ]HC-15 rat heart PET studies show rapid heart uptake to give clear heart images. The rat heart PET blocking studies found no significant blocking effect. The dynamic PET studies in normal and ablated dogs were performed using Siemens PET scanner with [ $^{13}\text{N}$ ]NH<sub>3</sub>, [ $^{11}\text{C}$ ]HC-15, and [ $^{18}\text{F}$ ]HC-15. PET studies in dogs of both [ $^{11}\text{C}$ ]HC-15 and [ $^{18}\text{F}$ ]HC-15 also show significant heart uptake and give images of the heart. However, there is no significant change in [ $^{11}\text{C}$ ]HC-15 L-ventricle uptake following radiofrequency ablation in the dog. These results suggest that the localization of HC-15 tracers in the heart is mediated by non-specific processes, and the visualization of HC-15 tracers on the heart is related to non-specific binding of HACU.  
© 2006 Elsevier Ltd. All rights reserved.

## 1. Introduction

Cardiac autonomic nervous system dysfunction plays a significant role in the genesis of ventricular tachyarrhythmias and sudden cardiac death in patients who have coronary heart disease.<sup>1</sup> Non-invasive imaging of heart autonomic nervous system is an active area of current molecular imaging research.<sup>2</sup> Radiotracer methods using biomedical imaging modalities such as positron emission tomography (PET) for heart imaging have been extensively investigated and validated.<sup>3</sup> In our pre-

vious work, we have synthesized and studied a series of PET heart imaging agents that target either sympathetic or parasympathetic nerve such as [ $^{11}\text{C}$ ]meta-hydroxyephedrine ([ $^{11}\text{C}$ ]HED), 5-[ $^{11}\text{C}$ ]methoxybenzovesamicol ([ $^{11}\text{C}$ ]MOBV), [ $^{11}\text{C}$ ]neostigmine, [ $^{11}\text{C}$ ]edrophonium, [ $^{11}\text{C}$ ]pyridostigmine, and *N*-[ $^{11}\text{C}$ ]methyl-3-[[dimethylamino]carbonyloxy]-2-(2',2'-diphenylpropionoxymethyl)pyridinium triflate ([ $^{11}\text{C}$ ]MDDP).<sup>4–9</sup> In this ongoing study, we targeted high-affinity choline uptake (HACU) system in the heart autonomic nervous system and developed radiolabeled hemicholinium-15 (HC-15) derivatives as new in vivo tracers for HACU system. The HACU system is located specifically in presynaptic cholinergic nerve terminals and was found to be the regulating and rate-limiting step in the synthesis of acetylcholine, thus, it is a biomarker of the functional status of the cholinergic presynaptic terminals.<sup>10</sup> Like

**Keywords:** [ $^{11}\text{C}$ ]Hemicholinium-15; [ $^{18}\text{F}$ ]Hemicholinium-15; Positron emission tomography; Heart imaging; High-affinity choline uptake.

\* Corresponding author. Tel.: +1 317 278 4671; fax: +1 317 278 9711; e-mail: [qzheng@iupui.edu](mailto:qzheng@iupui.edu)

hemicholinium-3 (HC-3), a golden standard for studying the HACU system in vitro, HC-15 is an inhibitor of HACU and is one-half of the molecule of HC-3 with similar in vitro affinity of potent HC-3.<sup>11</sup> To study HACU system in vivo, we proposed to develop radiolabeled HC-3 and HC-15 derivatives as PET probes. Because HC-3 is a bis-quaternary ammonium salt, it is relatively difficult to radiolabel. Thus, we synthesized radiolabeled HC-15 derivatives first. HC-15 labeled with a positron emitting radionuclide either carbon-11 or fluorine-18 may enable non-invasive monitoring of HACU system in the heart to study cardiac parasympathetic innervation using PET imaging technique. We present here our initial investigation on synthesis, biodistribution, and PET imaging of [<sup>11</sup>C]hemicholinium-15 ([<sup>11</sup>C]HC-15) and [<sup>18</sup>F]hemicholinium-15 ([<sup>18</sup>F]HC-15) as new potential in vivo heart HACU system biomarkers.

## 2. Results and discussion

### 2.1. Chemistry and radiochemistry

The precursor 4-methyl-2-phenyl-morpholin-2-ol (**3**) was synthesized from phenacyl bromide with 2-(methylamino)ethanol in 90% yield.<sup>12</sup> The methylation of compound **3** with methyl iodide provided HC-15 standard, 4,4-dimethyl-2-hydroxy-2-phenylmorpholinium iodide (**1a**), in 92% yield. The one-step reaction of phenacyl bromide with 2-(dimethylamino)ethanol provided another HC-15 standard, 4,4-dimethyl-2-hydroxy-2-phenylmorpholinium bromide (**1b**), in 95% yield.<sup>13</sup> The fluoromethyl-HC-15 standard, 4-(fluoromethyl)-2-hydroxy-4-methyl-2-phenylmorpholinium chloride (**2**), was prepared from the reaction of precursor **3** with a fluoromethylated agent, chlorofluoromethane, in 10% yield using a modification of the literature procedure.<sup>14</sup>

[<sup>11</sup>C]HC-15 was prepared by *N*-[<sup>11</sup>C]methylation of the precursor **3** using a reactive [<sup>11</sup>C]methylating agent, [<sup>11</sup>C]methyl triflate ([<sup>11</sup>C]CH<sub>3</sub>OTf),<sup>15</sup> and isolated by a simplified solid-phase extraction (SPE) method<sup>16</sup> in 55–70% decay corrected radiochemical yields based on [<sup>11</sup>C]CO<sub>2</sub>, 10–15 min overall synthesis time from end of bombardment (EOB), >99% radiochemical purity, and 2–3 Ci/μmol specific activity at end of synthesis (EOS). Either SiO<sub>2</sub> or cation-exchange CM Sep-Pak cartridge was used in SPE purification technique.

Similarly, [<sup>18</sup>F]HC-15 was prepared by *N*-[<sup>18</sup>F]fluoromethylation of the precursor **3** using a novel and reactive [<sup>18</sup>F]fluoromethylating agent, [<sup>18</sup>F]fluoromethyl triflate ([<sup>18</sup>F]FCH<sub>2</sub>OTf)<sup>17</sup>, followed by a fast SPE purification as mentioned above in 20–30% decay corrected radiochemical yields based on K[<sup>18</sup>F]F, 20–30 min overall synthesis time from EOB, >99% radiochemical purity, and >1.0 Ci/μmol specific activity at EOS.

The synthetic approach for the precursor, reference standards, and tracers is outlined in Scheme 1.

### 2.2. Tissue biodistribution studies

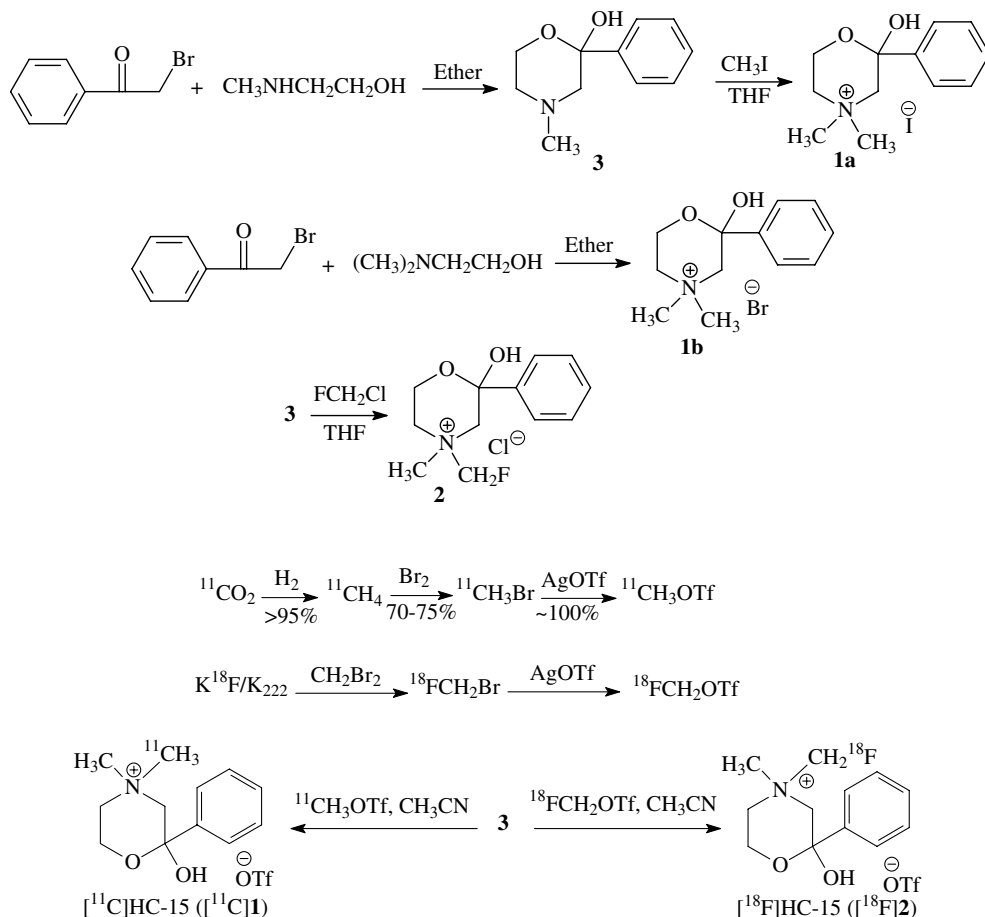
All animal experiments were performed under a protocol approved by the Indiana University (IU) Institutional Animal Care and Use Committee (IACUC). The in vivo biodistribution of [<sup>11</sup>C]HC-15 and [<sup>18</sup>F]HC-15 was determined in Fisher rats at 20 min post-intravenous (iv) injection, and the data are listed in Table 1. The heart region uptakes included L-atrium, R-atrium, septum, L-ventricle, R-ventricle, and A-V node. The significant heart ventricle uptakes were  $1.32 \pm 0.75\%$  ID/g in R-ventricle for [<sup>11</sup>C]HC-15 and  $1.28 \pm 0.81\%$  ID/g in L-ventricle for [<sup>18</sup>F]HC-15, respectively. The data presented here represented the average value in four rats. Highest uptakes were found in liver, kidney, and urine. Uptake in myocardial regions was moderate for both <sup>11</sup>C and <sup>18</sup>F tracers. In comparison with the uptakes in liver, kidney, and urine, the uptake in brain, blood, and muscle was very low. Both [<sup>11</sup>C]HC-15 and [<sup>18</sup>F]HC-15 are radiolabeled quaternary ammonium salts, therefore, it is not possible for the tracers to cross the blood–brain barrier (BBB). The biodistribution data of both tracers in brain confirmed the lipophilicity of the tracers,<sup>18</sup> which are consistent with their HPLC retention times.

### 2.3. Rat IndyPET-II imaging

Animal PET scanner, IndyPET-II, is a high-resolution (<3 mm full-width at half-maximum), high sensitivity, research PET scanner developed for small field-of-view (FOV) imaging applications including rodent imaging (mice, rats), intermediate size animals (dogs, pigs, primates), and dedicated human imaging applications (brain, breast).<sup>19,20</sup> In vivo dynamic PET imaging studies<sup>8,9</sup> of the tracer [<sup>11</sup>C]HC-15 in young adult female Sprague–Dawley rats were performed in the IndyPET-II scanner for 60 min post iv injection of 0.5–1.0 mCi of the tracer in a rat. Four rats were imaged. Each was imaged twice, once following iv injection in the tail vein with 3.0 mg/kg of unlabeled HC-15 in saline 30 min prior to tracer administration and imaging. Time between blocking injection and tracer injection was  $30 \pm 2$  min (mean  $\pm$  sd). Mean uptake values were calculated from region-of-interest (ROI) data for frames from 20 to 40 min following the start of the scans. Mean uptake values were analyzed with a mixed effect model taking the blocker as the fixed effect and the animal as a random effect.

A typical IndyPET-II coronal view image of [<sup>11</sup>C]HC-15 in a rat is shown in Figure 1. Image intensity is standard uptake value (SUV), averaged from 20 to 60 min after tracer injection. [<sup>11</sup>C]HC-15 rat heart PET dynamic studies show rapid heart uptake and blood pool clearance to give clear heart images.

The heart uptake normalized to injected dose/mass for the four rats (13, 14, 15, and 16) was studied. Data from blocked images are plotted as filled circles, while unblocked data are plotted as open circles. Except for rat 15, there is no effect. The *p* value from a mixed effect



**Scheme 1.** Synthesis of HC-15 precursor, reference standards, and tracers [ $^{11}\text{C}$ ]HC-15 and [ $^{18}\text{F}$ ]HC-15.

**Table 1.** Biodistribution data of [ $^{11}\text{C}$ ]HC-15 and [ $^{18}\text{F}$ ]HC-15 in Fisher rat model (%ID/g) at 20 min post iv injection

Organ	[ $^{11}\text{C}$ ]HC-15 ( $n = 4$ )	[ $^{18}\text{F}$ ]HC-15 ( $n = 4$ )
Blood	0.181 ± 0.095	0.201 ± 0.048
Brain	0.022 ± 0.012	0.046 ± 0.023
Lung	1.302 ± 1.161	3.423 ± 1.510
Liver	6.284 ± 2.843	4.378 ± 2.613
Kidney	3.618 ± 1.810	11.651 ± 8.016
Urine	31.835 ± 12.119	17.434 ± 4.510
<i>Heart regions</i>		
L-Atrium	0.526 ± 0.320	0.796 ± 0.304
R-Atrium	0.488 ± 0.222	0.756 ± 0.407
Septum	0.010 ± 0.005	1.557 ± 1.174
L-Ventricle	0.859 ± 0.494	1.280 ± 0.810
R-Ventricle	1.316 ± 0.750	0.037 ± 0.016
A-V Node	1.083 ± 1.016	0.793 ± 0.417
Solar plexus	0.938 ± 0.371	0.744 ± 0.212
Ske. musc.	0.091 ± 0.066	0.145 ± 0.063

The data presented here represented the average value in four rats.

model looking for effects from the blocking is 0.43, confirming what is clear from the graph. The initial PET blocking studies of [ $^{11}\text{C}$ ]HC-15 with pretreatment drug HC-15 in rats found only minor changes in rat heart [ $^{11}\text{C}$ ]HC-15 retention and no significant blocking in the data set. The left kidney uptake normalized to injected dose/mass for the four rats was studied. In the two

animals (13 and 16) where it was possible to see the kidney, there appears to be a significant blocking effect. Since there are missing data, this sample is too small to do a mixed effect calculation. A simple *t* test comparing blocked to unblocked gives a *p* value of 0.35, showing an insignificant result. The liver uptake normalized to injected dose/mass for the four rats was studied. Filled points were blocked with HC-15. Open points were not blocked. These data shows a significant blocking effect with a *p* value of 0.035. PET imaging studies in rats indicated a significant accumulation of radiotracer in the liver. This may be caused by the lipophilicity of the quaternary ammonium tracer aforementioned. Heart uptake (A), left kidney uptake (B), and liver uptake (C) of [ $^{11}\text{C}$ ]HC-15 in mean ROI intensity  $\times$  injected dose/mass  $\times 10^6$  within 60 min scan time using the IndyPET-II scanner in a representative study in rat 13 are shown in Figure 2. From the graphs in Figure 2, we can see the liver uptake is likely 5–10 times of the heart uptake, which is consistent with their biodistribution data as indicated in Table 1. The data are disappointing for the purpose of demonstrating specificity of the heart uptake, and thus we conclude that rat may not be a good model for evaluation of these type compounds in the heart.

#### 2.4. Canine PET imaging

Previous work from our laboratory has shown that parasympathetic fibers run along the left ventricular

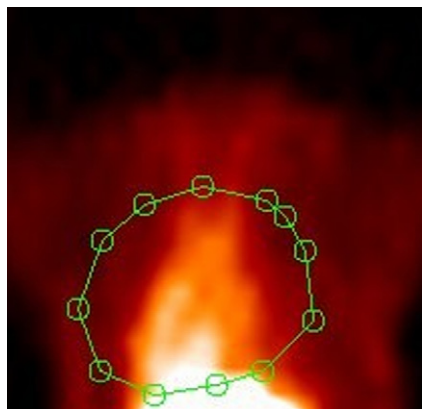


**Figure 1.** A coronal view image of  $[^{11}\text{C}]\text{HC-15}$  distribution in a rat acquired with the IndyPET-II scanner for 60 min. A green line surrounds the heart region. Image intensity is SUV averaged from 20 to 60 min after tracer injection.

endocardial surface.<sup>21</sup> Electroanatomic mapping and radiofrequency ablation (RFA) catheter techniques applied to the dog generated canine parasympathetic denervation model.<sup>22</sup> To further determine the exact binding site of the HC-15 tracers, dog PET imaging studies were performed. PET baseline images of  $[^{13}\text{N}]\text{NH}_3$ ,  $[^{11}\text{C}]\text{HC-15}$ , and  $[^{18}\text{F}]\text{HC-15}$  in a normal dog are shown in Figure 3. The images on the left-hand side are short-axis (SA) slices, while those on the right are horizontal long-axis (HLA) slices. The color scales are approximately similar for the  $[^{13}\text{N}]\text{NH}_3$  and  $[^{11}\text{C}]\text{HC-15}$ , and the  $[^{18}\text{F}]\text{HC-15}$  color scale has been turned up to show the uptake. Both  $[^{13}\text{N}]\text{NH}_3$  and  $[^{11}\text{C}]\text{HC-15}$  show significant heart uptake and give clear heart images, while relatively low heart uptake was seen with  $[^{18}\text{F}]\text{HC-15}$ .

Due to the low uptake of  $[^{18}\text{F}]\text{HC-15}$  in the normal dog, only  $[^{13}\text{N}]\text{NH}_3$  and  $[^{11}\text{C}]\text{HC-15}$  were administered in the ablated dog.  $[^{13}\text{N}]\text{NH}_3$ -PET in the dog served as a reference imaging study for the blood flow. PET images of  $[^{13}\text{N}]\text{NH}_3$  in a dog before RFA and after RFA are shown in Figure 4. The first row images are at HLA view, the second row images are at vertical long-axis (VLA) view, and the third row images are at SA view. There is no significant change in the images before RFA and after RFA. Kinetics of  $[^{13}\text{N}]\text{NH}_3$  within 30 min scan time in a dog before RFA and after RFA for two ROIs on the anterior L-ventricle (LV) wall are shown in Figure 5. The open black circles are from the normal, pre-ablation scan, and the filled green circles are from the scan following the first ablation. The figure shows there is a slight increase in tracer uptake following RFA, but there is no significant change of the kinetics of  $[^{13}\text{N}]\text{NH}_3$  in a dog before RFA and after RFA.

PET images of  $[^{11}\text{C}]\text{HC-15}$  in a dog before RFA and after RFA at HLA, VLA, and SA views are shown in Figure 6. Likewise, there is no significant change in the images before RFA and after RFA. Kinetics of  $[^{11}\text{C}]\text{HC-15}$  within 90 min scan time in a dog pre- and post-ablation, and kinetics of  $[^{18}\text{F}]\text{HC-15}$  within 90 min scan time in the same normal dog are shown in

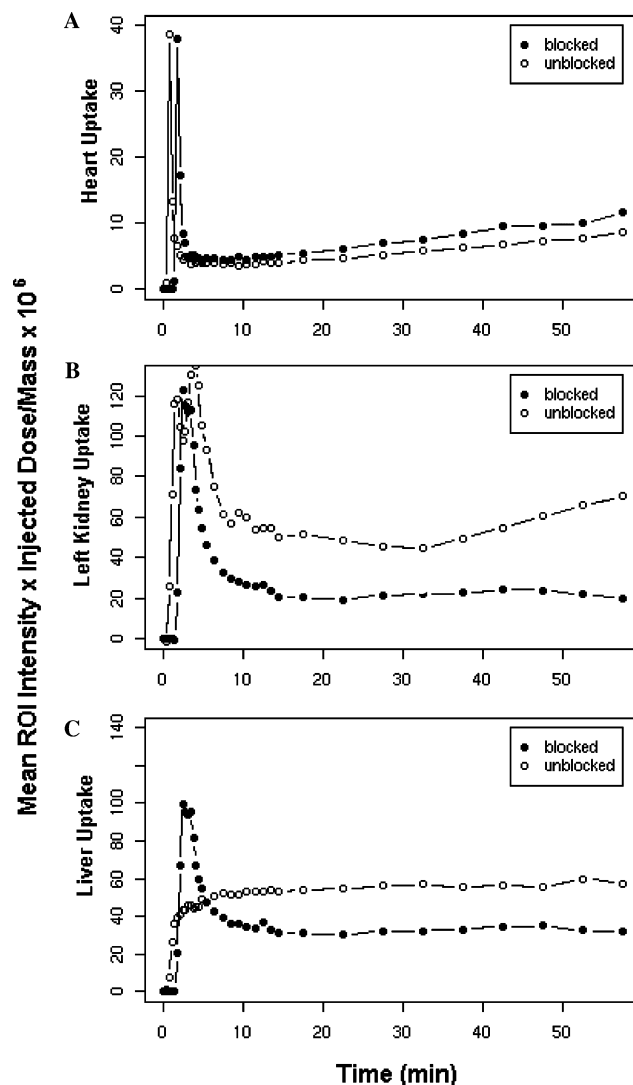


**Figure 2.** Heart uptake (A), left kidney uptake (B), and liver uptake (C) of  $[^{11}\text{C}]\text{HC-15}$  in mean ROI intensity  $\times$  injected dose/mass  $\times 10^6$  within 60 min scan time using the IndyPET-II scanner in a representative study in rat 13. Blocking of HACU was effected by pretreatment of rat with HC-15.

Figure 7. The open black (pre-ablation) and filled green (post-ablation) triangles are the  $[^{11}\text{C}]\text{HC-15}$  data, and the open black (pre-ablation) squares are the  $[^{18}\text{F}]\text{HC-15}$  data. Figure 7 shows that  $[^{11}\text{C}]\text{HC-15}$  has higher heart LV uptake than  $[^{18}\text{F}]\text{HC-15}$ , which is consistent with their PET images as shown in Figure 3, and there is no significant change of the kinetics in  $[^{11}\text{C}]\text{HC-15}$  LV uptake in the dog pre- and post-ablation.

### 3. Conclusion

In summary, the synthetic procedures for new C-11 and F-18 labeled HC-15 tracers have been well developed. Biodistribution studies show both  $[^{18}\text{F}]\text{HC-15}$  and  $[^{11}\text{C}]\text{HC-15}$  have certain uptakes in heart regions and would distribute to brain very little. Initial PET studies in blocked and unblocked rats demonstrate that myo-

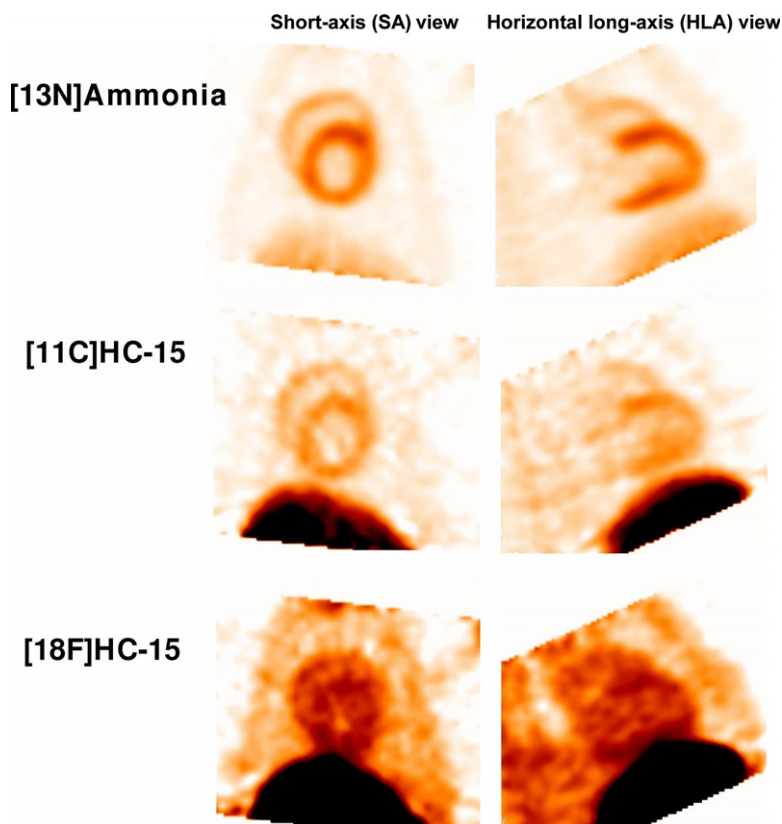


**Figure 3.** PET baseline images of  $[^{13}\text{N}]\text{NH}_3$ ,  $[^{11}\text{C}]\text{HC-15}$ , and  $[^{18}\text{F}]\text{HC-15}$  in a normal dog. The  $[^{13}\text{N}]\text{NH}_3$  images show homogeneous perfusion of the myocardium. Moderate uptake of  $[^{11}\text{C}]\text{HC-15}$  was observed throughout the myocardium, while relatively low myocardial uptake was seen with  $[^{18}\text{F}]\text{HC-15}$ .

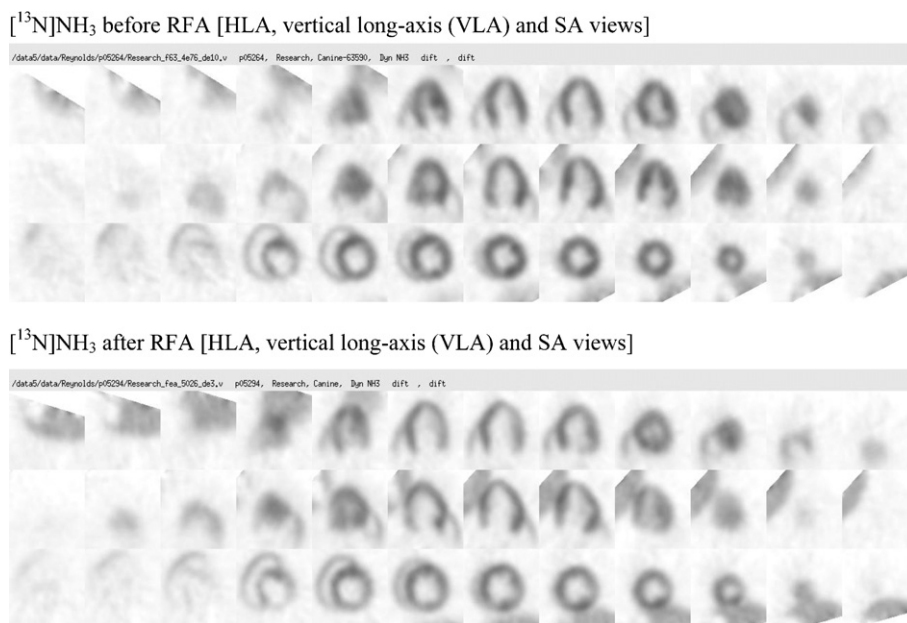


**Figure 4.** PET images of  $[^{13}\text{N}]\text{NH}_3$  in a dog before RFA and after RFA. There is no significant change in the images before RFA and after RFA.

cardial uptake of  $[^{11}\text{C}]\text{HC-15}$  is not blocked by HC-15 administration. Initial PET studies in normal and ablated dogs indicate there is no significant change in  $[^{13}\text{N}]\text{NH}_3$  or  $[^{11}\text{C}]\text{HC-15}$  LV uptake before RFA and after RFA—certainly nothing at all like that seen with

$[^{11}\text{C}]\text{HED}^4$  following denervation.  $[^{11}\text{C}]\text{HC-15}$  change is similar to  $[^{13}\text{N}]\text{NH}_3$  change, although it does slightly trend in the direction we expect if the tracer was indicating denervation. There is no evidence of an uptake defect coincident with the location of the ablation.

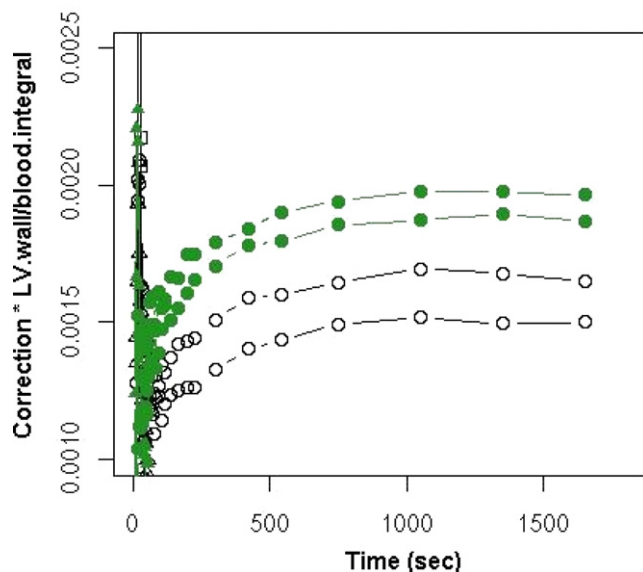


**Figure 5.** Kinetics of  $[^{13}\text{N}]\text{NH}_3$  within 30 min scan time in a dog pre-ablation scan and post-ablation scan. The plot shows the kinetics for  $[^{13}\text{N}]\text{NH}_3$  for two ROIs on the anterior LV wall. They are for the same dog. The open black circles are from the normal, pre-ablation scan, and the filled green circles are from the scan following the ablation. There is a slight increase in tracer uptake following RFA.

Taken collectively, these preliminary results suggest that the heart uptakes of the HC-15 tracers are most likely the result of non-specific binding. Therefore, we conclude the HC-15 compounds were unable to show specific binding of HACU, and the heart uptakes are due to non-specific binding. The reason that radiolabeled HC-15 compounds did not specifically bind to the HACU system might be related to their relatively low in vitro affinity in comparison with the really potent HC-3 compounds.<sup>11</sup> Among these HACU inhibitors, HC-3 should possess the combination of favorable phar-

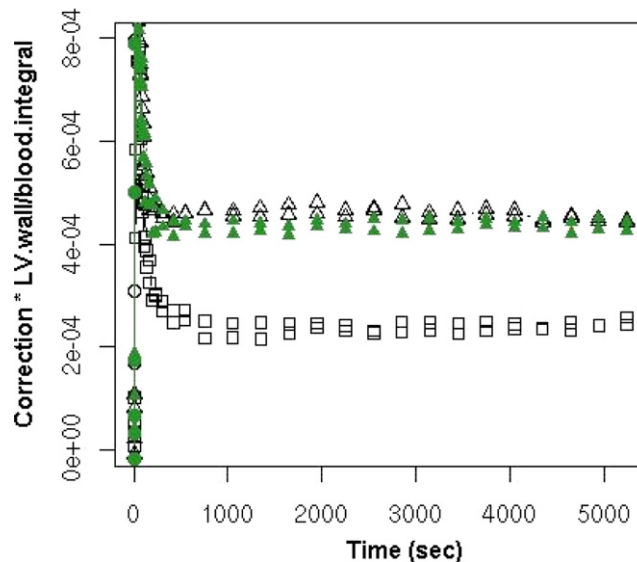


**Figure 7.** Kinetics of  $[^{11}\text{C}]\text{HC-15}$  and  $[^{18}\text{F}]\text{HC-15}$  within 90 min scan time in a dog. The triangles are the  $[^{11}\text{C}]\text{HC-15}$  data, and the squares are the  $[^{18}\text{F}]\text{HC-15}$  data. Black and green are as: pre- and post-RFA. The heart uptake of  $[^{11}\text{C}]\text{HC-15}$  is higher than that of  $[^{18}\text{F}]\text{HC-15}$ , and there is no significant change in  $[^{11}\text{C}]\text{HC-15}$  heart uptake following RFA.

macokinetics and more potent affinity for the HACU, since it represents at present the most potent known synthetic inhibitor of the HACU system. These same properties are often beneficial in a diagnostic radiotracer. To translate therapeutic agents for diagnostic use, our future works to develop HACU-specific, hemicholinium-based PET probes will be the in vivo biological evaluation of radiolabeled HC-3 derivatives,  $[^{11}\text{C}]\text{hemicholinium-3}$  ( $[^{11}\text{C}]\text{HC-3}$ ) and  $[^{18}\text{F}]\text{hemicholinium-3}$  ( $[^{18}\text{F}]\text{HC-3}$ ), to determine the exact binding site of the potent HACU inhibitors.

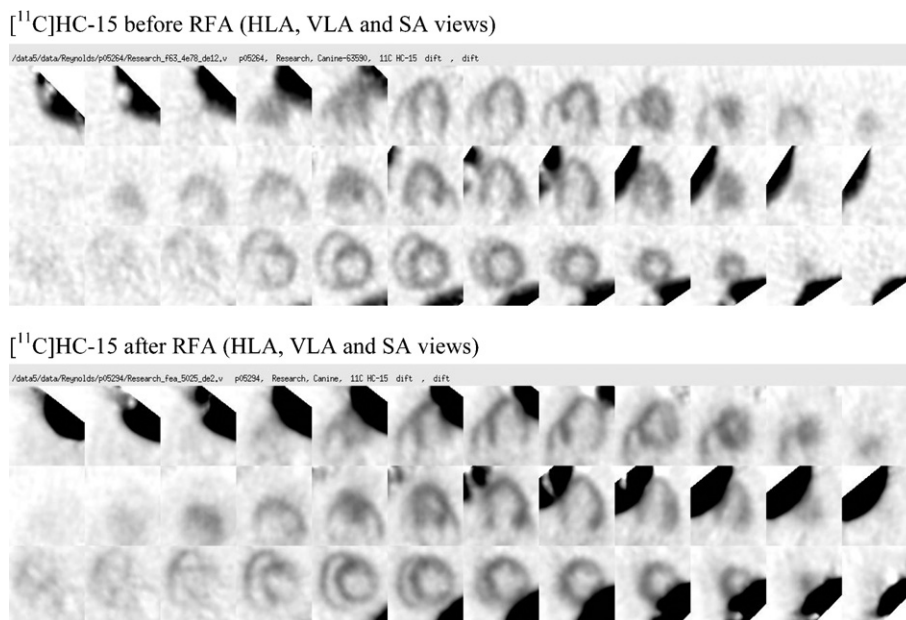


**Figure 6.** PET images of  $[^{11}\text{C}]\text{HC-15}$  in a dog before RFA and after RFA. There is no significant change in the images before RFA and after RFA.

## 4. Experimental

### 4.1. General

All commercial reagents and solvents were used without further purification.  $[^{13}\text{C}]\text{CH}_3\text{OTf}$  was made according to a literature procedure.<sup>15</sup> Melting points were determined on a MEL-TEMP II capillary tube apparatus and are uncorrected.  $^1\text{H}$  NMR spectra were recorded on a Bruker QE 300 FT-NMR spectrometer using tetramethylsilane (TMS) as an internal standard. Chemical shift data for the proton resonances were reported in parts per million (ppm,  $\delta$  scale) relative to internal standard TMS ( $\delta$  0.0), and coupling constants ( $J$ ) are reported in hertz (Hz). The low-resolution mass spectra (LRMS) were obtained using a Bruker Biflex III MALDI-TOF mass spectrometer, and the high-resolution mass spectra (HRMS) were obtained using a Kratos MS80 mass spectrometer. Chromatographic solvent proportions are expressed on a volume: volume basis. Thin-layer chromatography was run using Analtech silica gel GF uniplates ( $5 \times 10 \text{ cm}^2$ ). Plates were visualized by UV light. Normal phase flash chromatography was carried out on EM Science silica gel 60 (230–400 mesh) with a forced flow of the indicated solvent system in the proportions described below. All moisture- and/or air-sensitive reactions were performed under a positive pressure of nitrogen maintained by a direct line from a nitrogen source.

Analytical HPLC was performed using a Prodigy (Phenomenex)  $5 \mu\text{m}$  C-18 column,  $4.6 \times 250 \text{ mm}^2$ ; 3:1:3  $\text{CH}_3\text{CN}:\text{MeOH}:\text{20 mM}$ , pH 6.7  $\text{KHPO}_4^-$  (buffer solution) mobile phase; flow rate 1.5 mL/min; and UV (254 nm) and  $\gamma$ -ray (NaI) flow detectors. Semi-prep  $\text{SiO}_2$  Sep-Pak cartridge and cation-exchange CM Sep-Pak cartridge were obtained from Waters Corporate Headquarters, Milford, MA. Sterile Millex-GS 0.22  $\mu\text{m}$  vented filter unit was obtained from Millipore Corporation, Bedford, MA.

### 4.2. Synthesis of precursors and reference standards

**4.2.1. 4-Methyl-2-phenyl-morpholin-2-ol (3).** Compound **3** was synthesized using a modification of the literature method.<sup>12</sup> Phenacyl bromide (19.9 g, 0.10 mol) was dissolved in ether (200 mL) and added dropwise with stirring to 2-(methylamino)ethanol (15.2 g, 0.20 mol), which was dissolved in ether (180 mL). The mixture was stirred at room temperature for 24 h. The supernatant liquid was decanted or filtered from the precipitated *N*-substituted ethanolamine hydrobromide, washed with brine ( $3 \times 100 \text{ mL}$ ), and dried over  $\text{MgSO}_4$ . The solution was concentrated to give low melting point solid compound **3** (17.3 g, 90%),  $R_f = 0.76$  (1:9,  $\text{MeOH}/\text{CH}_2\text{Cl}_2$ ), mp 51–52 °C.  $^1\text{H}$  NMR (300 MHz,  $\text{CDCl}_3$ )  $\delta$ : 2.16–2.56 (m, 2H,  $\text{CH}_2$ ), 2.29 (s, 3H,  $\text{CH}_3$ ), 2.77 (dd,  $J = 11.1$ , 20.2 Hz, 2H,  $\text{CH}_2$ ), 3.82 (dd,  $J = 2.9$ , 11.8 Hz, 1H, *CHH*), 4.23 (dt,  $J = 2.9$ , 11.8 Hz, 1H, *CHH*), 4.74 (s, 1H, OH), 7.31–7.38 (m, 3H, Ph-H), 7.62 (dd,  $J = 1.7$ , 8.1 Hz, 2H, Ph-H).

**4.2.2. 4,4-Dimethyl-2-hydroxy-2-phenylmorpholinium iodide (1a).** To a solution of compound **3** (1.93 g,

10 mmol) in anhydrous tetrahydrofuran (THF, 40 mL) was added iodomethane (2.13 g, 15 mmol). The mixture was stirred at room temperature for 8 h, during the time a white solid precipitated. Then the solid was isolated by filtration, washed with THF ( $2 \times 5 \text{ mL}$ ), and dried under vacuum to provide compound **1a** as a white solid (3.08 g, 92%), mp 183–185 °C.  $^1\text{H}$  NMR (300 MHz,  $\text{DMSO}-d_6$ )  $\delta$ : 3.15 (s, 3H,  $\text{CH}_3$ ), 3.26 (d,  $J = 13.2$  Hz, 1H, *CHH*), 3.43 (s, 3H,  $\text{CH}_3$ ), 3.56 (d,  $J = 5.1$ , 2H,  $\text{CH}_2$ ), 3.62 (d,  $J = 13.2$ , 1H, *CHH*), 4.08 (d,  $J = 12.5$  Hz, 1H, *CHH*), 4.38–4.47 (m, 1H, *CHH*), 7.33 (d,  $J = 1.5$ , 1H, OH), 7.41–7.47 (m, 3H, Ph-H), 7.55–7.58 (m, 2H, Ph-H).

**4.2.3. 4,4-Dimethyl-2-hydroxy-2-phenylmorpholinium bromide (1b).** Compound **1b** was synthesized using a modification of the literature method.<sup>13</sup> Phenacyl bromide (6.22 g, 31.2 mmol) and 2-(dimethylamino)ethanol (2.78 g, 31.2 mmol) were added into dry ether (200 mL), stirred at room temperature for 24 h. A white solid was precipitated, filtered, and washed with dry ether ( $2 \times 20 \text{ mL}$ ) to give compound **1b** (8.54 g, 95%), mp 187–188 °C.  $^1\text{H}$  NMR (300 MHz,  $\text{DMSO}-d_6$ )  $\delta$ : 3.16 (s, 3H,  $\text{CH}_3$ ), 3.26 (d,  $J = 12.5$  Hz, 1H, *CHH*), 3.43 (s, 3H,  $\text{CH}_3$ ), 3.57 (d,  $J = 5.9$ , 2H,  $\text{CH}_2$ ), 3.63 (d,  $J = 13.2$ , 1H, *CHH*), 4.07 (d,  $J = 12.5$  Hz, 1H, *CHH*), 4.36–4.46 (m, 1H, *CHH*), 7.32 (d,  $J = 1.5$ , 1H, OH), 7.39–7.45 (m, 3H, Ph-H), 7.56 (dd,  $J = 1.8$ , 7.7 Hz, 2H, Ph-H).

**4.2.4. 4-(Fluoromethyl)-2-hydroxy-4-methyl-2-phenylmorpholinium chloride (2).** To a 50 mL pressure tube containing anhydrous THF (15 mL) at  $-45 \text{ }^\circ\text{C}$  was added compound **3** (0.50 g, 2.6 mmol), chlorofluoromethane (Synquest Labs, Alachua, FL) was bubbled through the solution for 20 min. Then the tube was sealed. The mixture was allowed to slowly warm to room temperature, stirred for 60 h, during the time a white solid precipitated. The solid was filtered, washed with dry THF (2 mL), and dried under vacuum to provide compound **2** as a white solid (68 mg, 10%), mp 153–155 °C.  $^1\text{H}$  NMR (300 MHz,  $\text{DMSO}-d_6$ )  $\delta$ : 3.16–3.78 (m, 7H,  $2 \times \text{CH}_2$  and  $\text{CH}_3$ ), 4.05–4.18 (m, 1H, *CHH*), 4.42–4.52 (m, 1H, *CHH*), 5.46–5.62 (m, 1H, *FCHH*), 5.85–6.14 (m, 1H, *FCHH*), 7.40–7.63 (m, 6H, Ph-H and OH). LRMS (ESI): 226.1 ( $\text{M}^+$ , 100%). HRMS (ESI): Calcd for  $\text{C}_{12}\text{H}_{17}\text{O}_2\text{NF}$  226.1237. Found 226.1229.

### 4.3. Synthesis of target tracers

**4.3.1.  $[^{13}\text{C}]\text{Hemicholinium-15}$  ( $[^{13}\text{C}]\text{HC-15}$ ,  $[^{13}\text{C}]\text{1}$ ).** Precursor **3** (0.1–0.2 mg) was dissolved in acetonitrile (250  $\mu\text{L}$ ). The mixture was placed in a sealed reaction vessel. No carrier-added (high specific activity)  $[^{13}\text{C}]\text{CH}_3\text{OTf}$  was passed through the reaction solution, which was cooled at  $\sim 0 \text{ }^\circ\text{C}$ , until radioactivity reached a maximum ( $\sim 3 \text{ min}$ ), and then the reaction mixture was heated at 80 °C for 5 min. The reaction tube was connected to the  $\text{SiO}_2$  Sep-Pak or CM Sep-Pak. The labeled product mixture solution was passed onto the Sep-Pak cartridge for SPE purification by gas pressure. The reaction vessel and Sep-Pak cartridge were washed with eth-

anol (5 mL) and water (2 mL), and the washing solution was discarded to a waste bottle. The final product [ $^{11}\text{C}$ ]1 was eluted from the  $\text{SiO}_2$  Sep-Pak with 90:8:2  $\text{H}_2\text{O}$ /EtOH/HOAc (2–4 mL) or the CM Sep-Pak with saline (2–4 mL) and sterile-filtered through a 0.22  $\mu\text{m}$  cellulose acetate membrane and collected into a sterile vial. The pH of the production solution from the  $\text{SiO}_2$  Sep-Pak was adjusted to 5.5–7.0 with 8.4%  $\text{NaHCO}_3$  solution (0.2–0.4 mL). Total radioactivity was assayed and the total volume (2.5–5.0 mL) was noted. The overall synthesis time was 10–15 min. The radiochemical yields decay corrected to EOB, from  $^{11}\text{CO}_2$ , were 55–70%, the radiochemical purity was >99%, and the chemical purity of the target tracer was >95% measured by analytical HPLC. Retention times in the analytical HPLC system were:  $t_{\text{R } 3} = 2.38$  min,  $t_{\text{R } 1} = 1.78$  min,  $t_{\text{R } [^{11}\text{C}]1} = 1.78$  min.

**4.3.2. [ $^{18}\text{F}$ ]Hemicholinium-15 ([ $^{18}\text{F}$ ]HC-15, [ $^{18}\text{F}$ ]2).** Precursor **3** (0.6–1.0 mg) was dissolved in acetone (0.6 mL), and the mixture was placed in a sealed reaction vessel. No carrier-added (high specific activity) [ $^{18}\text{F}$ ]fluoromethyl bromide prepared by a literature method<sup>23</sup> was passed through a silver triflate column at 200 °C to form [ $^{18}\text{F}$ ]FCH<sub>2</sub>OTf.<sup>17</sup> [ $^{18}\text{F}$ ]FCH<sub>2</sub>OTf was trapped in the reaction solution, and then the reaction mixture was heated at 40 °C for 10 min. The subsequent purification will be the same as above for the tracer [ $^{11}\text{C}$ ]1 to provide the final product [ $^{18}\text{F}$ ]2. The overall synthesis time was 20–30 min. The radiochemical yields decay corrected to EOB were 20–30%. Retention times in the analytical HPLC system were:  $t_{\text{R } 3} = 2.38$  min,  $t_{\text{R } 2} = 1.80$  min,  $t_{\text{R } [^{18}\text{F}]2} = 1.80$  min.

#### 4.4. Biodistribution

The Fisher rats (200–300 g) were injected intravenously with sub-pharmacologic doses (1–3 mCi) of [ $^{11}\text{C}$ ]HC-15 and [ $^{18}\text{F}$ ]HC-15 via the tail vein while under conscious restraint. At 20 min post-injection, rats were sacrificed by decapitation under halothane anesthesia, their tissues quickly excised, weighed, and the decay-corrected radioactive content measured using a Packard Cobra Quantum gamma counter. The results are expressed as percentage of injected dose (%ID) and as percentage of injected dose per mass of tissue (%ID/g). For calculation of total blood activity, blood mass was assumed to be 7% of the body mass.

#### 4.5. Rat PET imaging

The IndyPET-II scanner designed and developed within IU PET facility<sup>19,20</sup> was used for rat PET imaging studies. The young adult female Sprague–Dawley rat (250–300 g) was anesthetized with acepromazine (0.2 mg/kg, im) and torbugesic (0.2 mg/kg, im). 0.5–1.0 mCi of [ $^{11}\text{C}$ ]HC-15 was administered intravenously to the rat via the tail vein. The PET images of the tracer were acquired in IndyPET-II scanner by the ordered subsets expectation maximization (OSEM) using 6 subsets/4 iterations for 60 min dynamic scans from a rat post iv injection of 0.5 mCi of the tracer, and

frame durations were defined as 300 s for entire 3600 s scan. For the blocking experiments, the rats were pretreated by iv injection in the tail vein with 3.0 mg/kg of unlabeled HC-15 cold drug in saline 30 min prior to iv injection of 0.5 mCi [ $^{11}\text{C}$ ]HC-15 in the tail vein. After tracer administration, the animals were handled as described above.

#### 4.6. Dog denervation procedure

Mongrel dogs (20–30 kg) were premedicated with morphine sulfate (2 mg/kg, im) and cephazolin sodium (3 mg/kg, im), and anesthetized with sodium thiopental (25 mg/kg, iv). A cuffed endotracheal tube was inserted and anesthesia was maintained with 1–3% isoflurane. The right groin was shaved and scrubbed with betadine and alcohol. Sterile surgical technique was followed throughout the procedure. An 8 French arterial sheath was placed in right femoral artery using the modified Seldinger technique. An electroanatomic mapping and RFA catheter (CARTO BioSense<sup>®</sup>) was placed in left ventricle, with creation of nearly circumferential line of ablation approximately 1 cm below the atrioventricular groove,<sup>22</sup> avoiding the area of cardiac bundle branches. Eighty-seven applications of RFA were used to create line of ablation, with disruption of endocardial electrical conduction confirmed after ablation completed. After a 5–7 day recovery period, repeat PET imaging was performed to re-assess the degree of parasympathetic innervation. The tracer kinetic models were employed in these studies to produce indices of regional choline transporter levels in the heart. The denervation procedure was performed at IU Krannert Institute of Cardiology clean procedure room and catheterization laboratory and was approved by the institutional IACUC.

#### 4.7. Canine PET imaging

The Siemens CTI EXACT HR+ PET scanner at IU PET facility was used for the canine PET imaging studies. A normal Mongrel dog underwent 30-min dynamic PET imaging with [ $^{13}\text{N}$ ]NH<sub>3</sub> for myocardial blood flow, and 90-min dynamic PET imaging with [ $^{11}\text{C}$ ]HC-15 and [ $^{18}\text{F}$ ]HC-15 for baseline imaging studies. The same dog before RFA and after RFA received 30-min dynamic PET scan with [ $^{13}\text{N}$ ]NH<sub>3</sub> to image myocardial blood flow, and 90-min dynamic PET scan with [ $^{11}\text{C}$ ]HC-15 to image parasympathetic nerve endings.

#### Acknowledgments

This work was partially supported by the Donald W. Reynolds Foundation and the Indiana Genomics Initiative (INGEN) of Indiana University, which is supported in part by Lilly Endowment Inc. The authors thank Shuyan Wang, Kevin Perry, Susan Giger, and Tanya Martinez for their assistance in animal studies, and Barbara Glick-Wilson and Michael Sullivan for their assistance in the production of radiolabeled precursors

$^{11}\text{CH}_3\text{OTf}$  and  $\text{K}^{18}\text{F/Kryptofix2.2.2}$ . The referees' criticisms and editor's comments for the revision of the manuscript are greatly appreciated.

### References and notes

1. Paul-Labrador, M.; Polk, D.; Dwyer, J. H.; Velasquez, I.; Nidich, S.; Rainforth, M.; Schneider, R.; Merz, C. N. *Arch. Intern. Med.* **2006**, *166*, 1218.
2. Knuuti, J.; Sipola, P. *Q. J. Nucl. Med. Mol. Imaging* **2005**, *49*, 97.
3. Bengel, F. M.; Schwaiger, M. *J. Nucl. Cardiol.* **2004**, *11*, 603.
4. Hutchins, G. D.; Chen, T.; Carlson, K. A.; Fain, R. L.; Winkle, W.; Vavrek, T.; Mock, B. H.; Zipes, D. P. *J. Nucl. Med.* **1999**, *40*, 846.
5. Olgin, J. E.; Sih, H. J.; Hanish, S.; Jayachandran, J. V.; Wu, J.; Zheng, Q.-H.; Winkle, W.; Mulholland, G. K.; Zipes, D. P.; Hutchins, G. *Circulation* **1998**, *98*, 2608.
6. Mulholland, G. K.; Zheng, Q.-H.; Mock, B. H.; Carlson, K. A.; Giger, S.; Vavrek, M. T.; Fain, R. L.; Hutchins, G. D. *J. Nucl. Med.* **1999**, *40*(5 Suppl. S), 495.
7. Zheng, Q.-H.; Liu, X.; Fei, X.; Wang, J.-Q.; Mock, B. H.; Glick-Wilson, B. E.; Sullivan, M. L.; Hutchins, G. D. *Bioorg. Med. Chem. Lett.* **2003**, *13*, 1787.
8. Wang, J.-Q.; Miller, M. A.; Fei, X.; Stone, K. L.; Lopshire, J. C.; Groh, W. J.; Zipes, D. P.; Hutchins, G. D.; Zheng, Q.-H. *Nucl. Med. Biol.* **2004**, *31*, 957.
9. Wang, J.-Q.; Miller, M. A.; Mock, B. H.; Lopshire, J. C.; Groh, W. J.; Zipes, D. P.; Hutchins, G. D.; Zheng, Q.-H. *Bioorg. Med. Chem. Lett.* **2005**, *15*, 4510.
10. Gilissen, C.; de Groot, T. J.; Bronfman, F.; van Leuven, F.; Verbruggen, A. M.; Bormans, G. M. *J. Nucl. Med.* **2003**, *44*, 269.
11. Smart, L. A. *J. Med. Chem.* **1983**, *26*, 104.
12. Cromwell, N. H.; Tsou, K.-C. *J. Am. Chem. Soc.* **1949**, *71*, 993.
13. Rekkas, E.; Kourounakis, P. *Eur. J. Med. Chem.* **1989**, *24*, 179.
14. DeGrado, T. R.; Coleman, R. E.; Wang, S.; Baldwin, S. W.; Orr, M. D.; Robertson, C. N.; Polascik, T. J.; Price, D. T. *Cancer Res.* **2001**, *61*, 110.
15. Mock, B. H.; Mulholland, G. K.; Vavrek, M. T. *Nucl. Med. Biol.* **1999**, *26*, 467.
16. Zheng, Q.-H.; Mock, B. H. *Biomed. Chromatogr.* **2005**, *19*, 671.
17. Iwata, R.; Pascali, C.; Bogoni, A.; Furumoto, S.; Terasaki, K.; Yanai, K. *Appl. Radiat. Isot.* **2002**, *57*, 347.
18. Liu, X.; Wang, J.-Q.; Zheng, Q.-H. *Biomed. Chromatogr.* **2005**, *19*, 379.
19. Frese, T.; Rouze, N. C.; Bouman, C. A.; Sauer, K.; Hutchins, G. D. *IEEE Trans. Med. Imaging* **2003**, *22*, 258.
20. Rouze, N. C.; Hutchins, G. D. *IEEE Trans. Nucl. Sci.* **2003**, *50*, 1491.
21. Takahashi, N.; Barber, M. J.; Zipes, D. P. *Am. J. Physiol.* **1985**, *248*, H89.
22. Kaseda, S.; Zipes, D. P. *Am. J. Physiol.* **1988**, *255*, H534.
23. DeGrado, T. R.; Baldwin, S. W.; Wang, S.; Orr, M. D.; Liao, R. P.; Friedman, H. S.; Reiman, R.; Price, D. T.; Coleman, R. E. *J. Nucl. Med.* **2001**, *42*, 1805.